International Journal of Environmental Sciences
ISSN: 2229-7359
Vol. 12 No. 1, 2026
https://theaspd.com/index.php

# Green Synthesis and Characterization of Zinc Oxide Nanoparticles Using Mentha aquatica Leaf Extract: Photocatalytic, Antibacterial, and Antioxidant Applications

**Nassima Ramdani**[1,2*], **Nadia Fekih**[1,3]

[1]Department of Material Science, Faculty of Science and Technology, University of Ain Temouchent, Ain Temouchent, 46000 Algeria.
[2]Applied Chemistry Laboratory, University of Ain Temouchent, Ain Temouchent, 46000 Algeria.
[3]Department of Chemistry, Faculty of Sciences, Laboratory for Natural and Bioactive Compounds (LASNABIO),
University of Tlemcen, Tlemcen, 13000 Algeria
*Corresponding author email: nassima.ramdani@univ-temouchent.edu.dz, chlouche2003@yahoo.fr

**Received:** 14/09/2025 **Accepted:** 17/04/2026 **Published:** 26/05/2026

***Abstract***

*This study reports the green synthesis of zinc oxide nanoparticles (ZnO NPs) using an aqueous extract of Mentha aquatica (water mint) leaves as a bio-reducing and capping agent. The synthesis was performed by the reduction of zinc acetate dihydrate [Zn(CH3COO)2·2H2O] in the presence of the plant extract under alkaline conditions and thermal treatment at 60 °C for 1 h, followed by calcination at 400 °C for 2 h. The resulting nanoparticles were characterized using UV-Vis spectrophotometry, Fourier Transform Infrared (FTIR) spectroscopy, X-ray diffraction (XRD), and Scanning Electron Microscopy (SEM). UV-Vis analysis revealed a characteristic absorption band at ~380 nm, confirming the formation of ZnO NPs. FTIR analysis identified the functional groups responsible for the bioreduction of zinc ions. XRD patterns confirmed the hexagonal wurtzite crystal structure of the synthesized particles, consistent with JCPDS card No. 36-1451, with principal diffraction peaks at 2θ values of 32.25°, 34.98°, and 36.79°. SEM images revealed spherical to granular morphologies with particle sizes in the range of 16–22 nm. The synthesized ZnO NPs exhibited excellent photocatalytic degradation of methylene blue (MB) dye under natural solar irradiation, achieving near-complete decolorization within 120 minutes. Disk diffusion assays demonstrated strong antibacterial activity against Gram-negative bacteria (E. coli: 35 mm inhibition zone; P. acip: 23 mm) and moderate activity against Gram-positive S. aureus (ATCC 43300: 15 mm). Antioxidant screening via the DPPH radical scavenging assay yielded an IC50 of 9.5 mg/mL for ZnO NPs, indicating moderate antioxidant potential. These results establish Mentha aquatica leaf extract as a promising, eco-friendly bio-template for ZnO NP synthesis with multifunctional applications.*

***Keywords:*** *Green synthesis; Zinc oxide nanoparticles; Mentha aquatica; Photocatalysis; Methylene blue; Antibacterial activity; DPPH antioxidant; Wurtzite structure*

## 1. INTRODUCTION

Nanotechnology has emerged as one of the most impactful fields of modern science, enabling the design and fabrication of materials with unique properties at the nanoscale. Among the various metal oxide nanoparticles studied, zinc oxide (ZnO) has attracted considerable attention due to its wide direct bandgap (~3.37 eV), large exciton binding energy (60 meV), non-toxicity, low cost, and remarkable versatility in photocatalysis, antimicrobial applications, and environmental remediation [1, 2].

Conventional physical and chemical synthesis routes for ZnO nanoparticles often involve hazardous reagents, high energy consumption, and generate toxic by-products, raising serious environmental and safety concerns. In response, green synthesis—using biological systems such as plant extracts, microorganisms, or agricultural waste—has emerged as a sustainable and cost-effective alternative [3]. Plant extracts are particularly attractive because they contain a rich repertoire of phytochemicals including phenolic acids, flavonoids, terpenoids, and alkaloids that function as natural reducing and capping agents, enabling the bio-fabrication of nanoparticles under mild conditions [4].

Mentha aquatica (water mint), a perennial herb of the Lamiaceae family, is abundant in polyphenolic compounds such as rosmarinic acid, luteolin, and various flavonoids, which endow its extract with potent reducing capability. In the context of green nanosynthesis, Mentha species have recently attracted interest as

bio-reducing templates for metal oxide nanoparticles [5]. For instance, Mentha piperita-derived ZnO NPs have been shown to display superior stability and bioactivity relative to chemically synthesized counterparts [6], and Mentha spicata extract has been used to produce well-defined ZnO NPs with potent antibacterial properties [7]. Photocatalytic degradation of organic dyes such as methylene blue (MB) using semiconductor ZnO NPs represents a promising strategy for wastewater treatment. Under solar irradiation, ZnO NPs generate electron-hole pairs that initiate radical-driven oxidation reactions capable of mineralizing persistent organic pollutants [8]. Additionally, ZnO NPs demonstrate broad-spectrum antibacterial activity, particularly against Gram-negative bacteria, through mechanisms involving reactive oxygen species (ROS) generation and membrane disruption [9].

This work aims to (i) synthesize ZnO NPs using an aqueous extract of Mentha aquatica leaves as a green reducing agent, (ii) perform comprehensive physicochemical characterization using UV-Vis, FTIR, XRD, and SEM, and (iii) evaluate the photocatalytic, antibacterial, and antioxidant performance of the synthesized nanoparticles.

## 2. MATERIALS AND METHODS

### 2.1 Plant Material and Extract Preparation

Fresh leaves of Mentha aquatica were collected, washed thoroughly with distilled water, and dried at ambient temperature. Twenty grams of dried leaves were boiled in 200 mL of distilled water for 30 min, filtered through Whatman No. 1 filter paper, and the clear aqueous extract was stored at 4 °C until use.

### 2.2 Green Synthesis of ZnO Nanoparticles

ZnO nanoparticles were synthesized by dissolving 0.5 g of zinc acetate dihydrate [Zn(CH3COO)2·2H2O, MW = 219.49 g/mol] in 50 mL of distilled water under constant magnetic stirring. Six milliliters of the Mentha aquatica leaf extract were added dropwise to the zinc acetate solution, followed by the gradual addition of 0.1 M NaOH solution until sediment formation was observed. The reaction mixture was maintained at 60 °C for 1 h under continuous magnetic stirring on a hot plate.

The resulting precipitate was collected by centrifugation at 4500 rpm for 10 min, washed three times with distilled water to remove residual phytochemicals, and dried overnight at 80 °C in an oven. The final ZnO NPs were obtained after calcination at 400 °C for 2 h in a muffle furnace to remove organic residues and improve crystallinity.

### 2.3 Characterization Techniques

UV-Vis absorption spectra were recorded using a double-beam spectrophotometer in the 350–800 nm wavelength range. FTIR spectra were acquired on a Perkin-Elmer spectrometer in the 4000–400 cm-1 range using KBr pellets. XRD patterns were obtained using a PANalytical X'Pert Pro diffractometer with CuKα radiation (λ = 0.15406 nm). The crystallite size was estimated using the Debye-Scherrer equation: $D = k\lambda/(\beta \cos \theta)$, where k is the shape factor (0.89), λ is the X-ray wavelength, β is the full width at half maximum (FWHM), and θ is the Bragg angle. SEM observations were performed on a JEOL scanning electron microscope operating at 15.0 kV.

### 2.4 Photocatalytic Activity

Photocatalytic degradation of methylene blue (MB, 10-5 M) was evaluated under natural solar irradiation. ZnO NPs (10 mg) were dispersed in 50 mL of the MB solution and stirred in the dark for 30 min to establish adsorption-desorption equilibrium. The reaction suspension was then exposed to sunlight for 120 min. Aliquots were withdrawn at regular intervals (30, 60, and 120 min), centrifuged, and the residual MB concentration was measured at 664 nm using UV-Vis spectroscopy.

### 2.5 Antibacterial Activity

The antibacterial activity of ZnO NPs was evaluated against four bacterial strains: E. coli (Gram-negative), P. acip (Gram-negative), S. aureus ATCC 25932 (Gram-positive), and S. aureus ATCC 43300 (Gram-positive) by the agar disk diffusion method. Mueller-Hinton agar plates were inoculated with each bacterial suspension (0.5 McFarland standard). Disks (6 mm diameter) loaded with 20 µL of ZnO NP suspension (1 mg/mL in DMSO) were placed on the agar surface, and inhibition zones were measured after 24 h incubation at 37 °C.

**2.6 Antioxidant Activity (DPPH Assay)**

Antioxidant activity was assessed using the 1,1-diphenyl-2-picrylhydrazyl (DPPH) free radical scavenging assay. Various concentrations of ZnO NPs (0–10 mg/mL) were mixed with 1 mL of 0.1 mM DPPH solution in ethanol and incubated in the dark at room temperature for 30 min. Absorbance was measured at 517 nm, and ascorbic acid (AA) was used as the positive control. Inhibition percentage was calculated as: % inhibition = [(A_control - A_sample) / A_control] × 100.

## 3. RESULTS AND DISCUSSION

### 3.1 UV-Vis Spectroscopy

The UV-Vis absorption spectrum of the as-synthesized ZnO NPs is presented in Figure 1. A pronounced absorption band is observed at approximately 380 nm, which is attributed to the characteristic intrinsic band gap absorption of ZnO arising from the electron transition from the O2p valence band to the Zn4s conduction band. This excitonic peak is in excellent agreement with values reported in the literature for green-synthesized ZnO NPs (typically 350–390 nm) [1, 3].

The presence of this band confirms the successful formation of ZnO nanoparticles through the bioreduction of Zn2+ ions by the phenolic compounds present in Mentha aquatica extract. Similar UV-Vis profiles have been reported for ZnO NPs synthesized from other Mentha species, with characteristic absorption maxima in the range of 360–385 nm [6, 7].

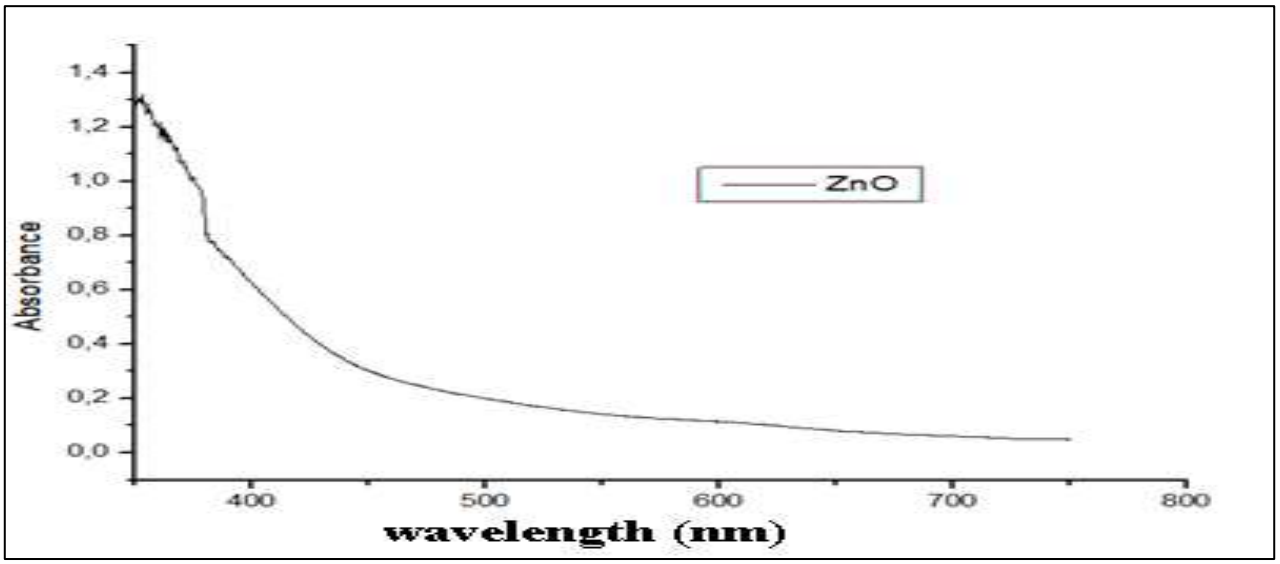


Figure 1. UV-Vis absorption spectrum of ZnO nanoparticles synthesized using Mentha aquatica leaf extract, showing the characteristic absorption band at ~380 nm.

### 3.2 FTIR Spectroscopy

The FTIR spectrum of Mentha aquatica-mediated ZnO NPs is shown in Figure 2. Several characteristic absorption bands are identified:

The broad absorption band at ~3228 cm-1 is assigned to O-H stretching vibrations of surface-adsorbed hydroxyl groups and polyphenolic phytochemicals. These hydroxyl groups from flavonoids and phenolic acids present in the mint extract are believed to coordinate with Zn2+ ions, facilitating their reduction and stabilization of the nanoparticle surface [4, 8].

The band at 1619 cm-1 corresponds to C=O carbonyl stretching vibrations of carboxylate groups derived from phenolic acids such as rosmarinic acid, which are characteristic capping agents in plant-mediated nanoparticle synthesis [9]. The absorption at ~1099 cm-1 is attributed to C-O stretching of polysaccharides and glycosidic groups. Crucially, the band at 628 cm-1 is characteristic of Zn-O stretching vibrations, confirming the successful formation of the ZnO crystalline phase [1, 2]. These results indicate that residual phytochemicals from the Mentha aquatica extract serve as effective capping and stabilizing agents on the nanoparticle surface.

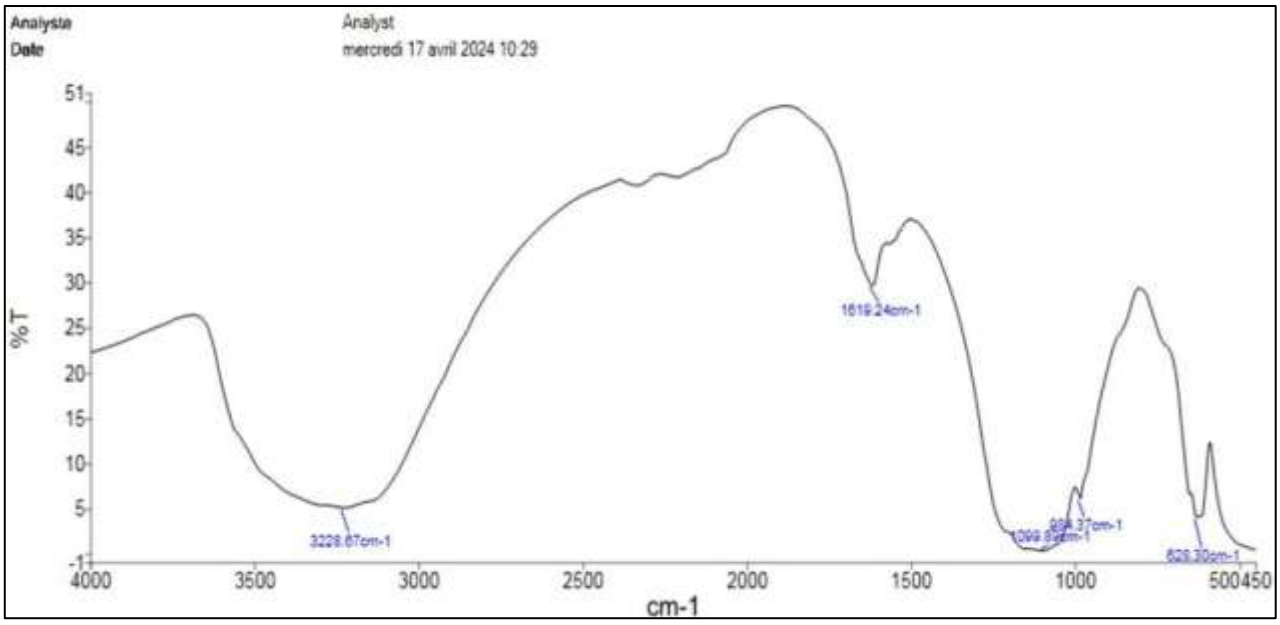


Figure 2. FTIR spectrum of ZnO nanoparticles synthesized using Mentha aquatica leaf extract. Key absorption bands are labeled (cm-1).

### 3.3 X-ray Diffraction (XRD) Analysis

The XRD pattern of the calcined ZnO NPs is displayed in Figure 3. Three intense diffraction peaks at 2θ values of 32.25°, 34.98°, and 36.79° corresponding to the (100), (002), and (101) crystal planes, respectively, confirm the formation of pure hexagonal wurtzite-structured ZnO (JCPDS card No. 36-1451). Additional diffraction peaks indexing to the (102), (110), (103), (200), (112), and (201) planes are also observed, with no detectable impurity phases, indicating high phase purity of the synthesized product.

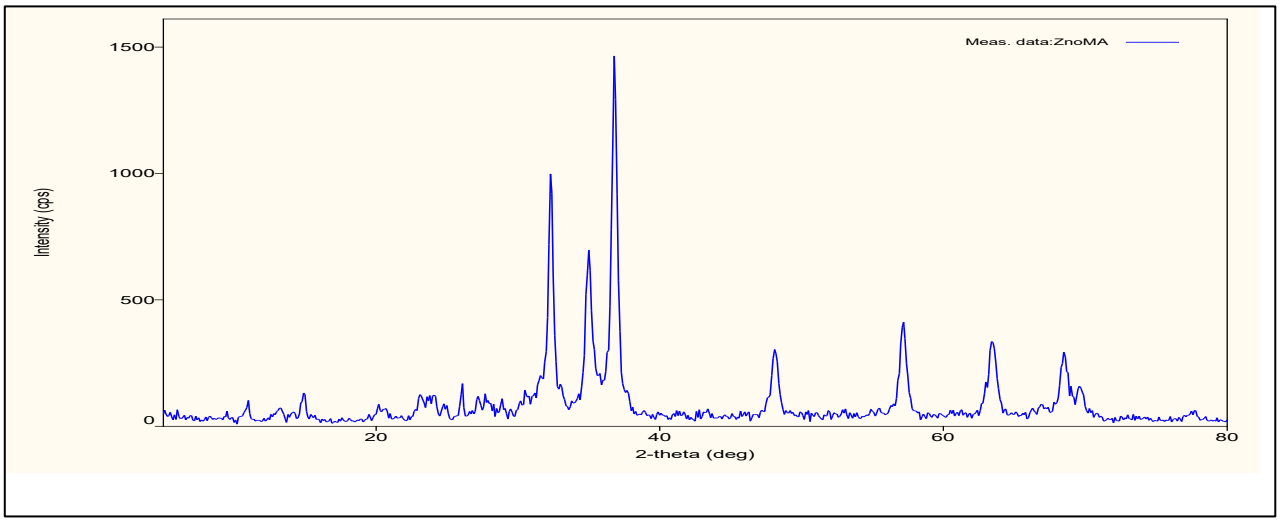


Figure 3: X-ray diffraction of ZnO nanoparticles.

The sharp and narrow diffraction peaks indicate good crystallinity of the nanoparticles. The crystallite size calculated using the Debye-Scherrer formula from the most intense (101) peak was estimated to be in the range of 16–22 nm, in good agreement with SEM observations (Section 3.4). These structural characteristics are consistent with recent reports on plant-extract-mediated ZnO NPs [3, 5, 8] and confirm that the calcination step effectively removed organic residues while promoting crystallization.

### 3.4 Scanning Electron Microscopy (SEM)

SEM images of the synthesized ZnO NPs are shown in Figure 4. The SEM micrographs reveal that the nanoparticles are predominantly spherical and granular in morphology, with individual particles as well as some aggregated clusters visible. The particle size distribution ranges from approximately 16 to 22 nm, as determined by measuring individual particles across multiple micrographs. Some degree of agglomeration is

observed, which is commonly reported for plant-mediated ZnO NPs and is attributed to the high surface energy of nanoscale particles as well as residual organic capping agents [2, 9].

The granular, well-dispersed morphology observed is consistent with previous reports on ZnO NPs synthesized using extracts of Moringa oleifera [10], Lupinus albus [11], and various Mentha species [6, 7], where similar size ranges (15–30 nm) and spherical morphologies were documented. The relatively small size and large specific surface area of the synthesized particles are advantageous for enhanced photocatalytic and antibacterial performance.

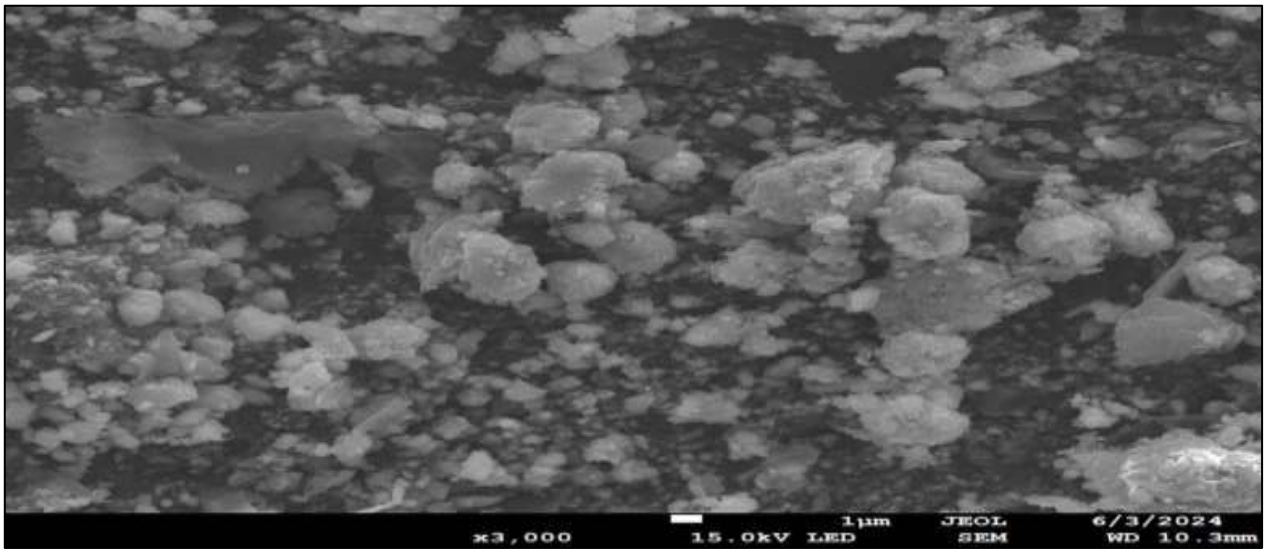


Figure 4. Scanning Electron Microscopy (SEM) image of ZnO nanoparticles synthesized from Mentha aquatica leaf extract (JEOL, 15.0 kV, ×3000 magnification, scale bar: 1 μm), confirming spherical-to-granular morphology and nanoscale particle size.

**4. Applications of ZnO Nanoparticles**

**4.1 Photocatalytic Degradation of Methylene Blue**

**4.1.1 Spectral Evolution**

The photocatalytic activity of the synthesized ZnO NPs was evaluated by monitoring the degradation of methylene blue (MB) dye under natural solar irradiation. Figure 5a presents the temporal evolution of the UV-Vis absorption spectra of MB solution ($\lambda_{max}$ = 664 nm) with and without ZnO NPs under solar exposure for 120 min.

In the absence of ZnO NPs (direct photolysis), only a minor reduction in MB absorbance was observed, confirming the limited self-degradation of MB under sunlight alone. In contrast, in the presence of ZnO NPs, the characteristic absorption peak of MB at 664 nm decreased progressively and substantially with increasing irradiation time. After 120 min, the MB absorption peak was nearly eliminated, indicating near-complete photodegradation. The corresponding color change from deep blue to nearly transparent is visually confirmed by the digital photographs in Figure 5b, demonstrating the practical effectiveness of ZnO NPs as solar photocatalysts.

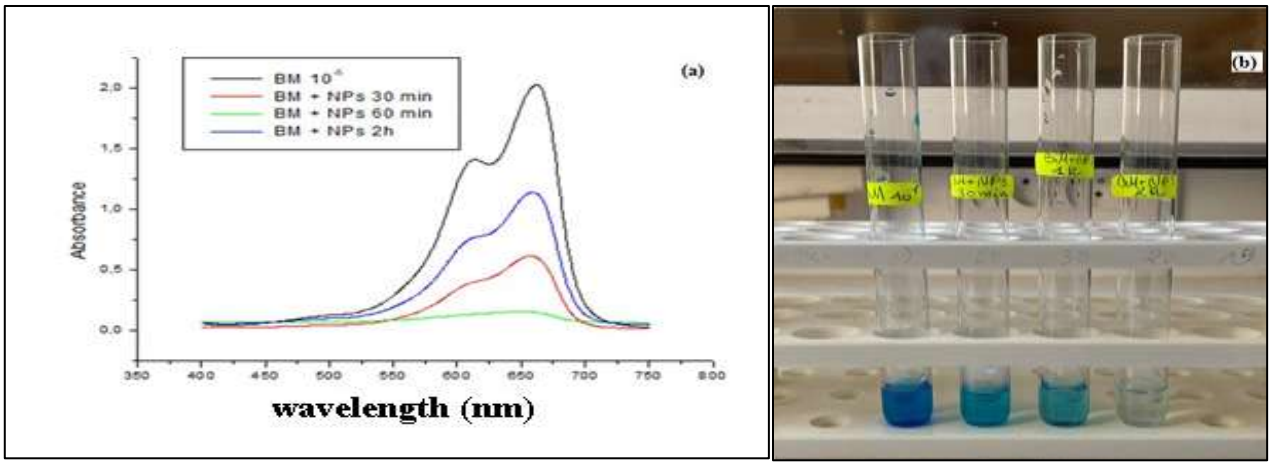


Figure 5. (a) Temporal UV-Vis absorption spectra showing progressive degradation of methylene blue (MB) by ZnO NPs under solar irradiation (BM 10-5 M, 30 min, 60 min, 2 h). (b) Digital photographs showing the visual color change of MB solution from deep blue to near-transparent as a function of irradiation time.

**4.1.2 Photocatalytic Mechanism**

The proposed photocatalytic mechanism for MB degradation by ZnO NPs under solar irradiation is illustrated in Figure 6. The mechanism proceeds through the following steps:

Upon absorption of photons with energy equal to or exceeding the band gap energy (Eg ≈ 3.3 eV), ZnO NPs undergo photo-excitation, generating electron-hole (e-/h+) pairs:

ZnO + hν → ZnO (eCB-) + ZnO (hVB+)

The photogenerated electrons (eCB-) react with dissolved O2 to form superoxide radicals (O2•-), while the holes (hVB+) react with surface OH- and H2O to produce hydroxyl radicals (OH•). These reactive oxygen species (ROS) attack the MB chromophore and auxochrome groups, ultimately mineralizing the dye to CO2 and H2O:

MB + OH• → CO2 + H2O + inorganic ions

This mechanism is fully consistent with the established photocatalytic pathway of ZnO-based semiconductor photocatalysts [8, 12, 13], where the rate of degradation is governed by the competition between charge carrier recombination and productive ROS formation. The efficiency observed in this study is attributed to the small particle size (16–22 nm), high surface area, and the preserved crystallinity of the Mentha aquatica-derived ZnO NPs.

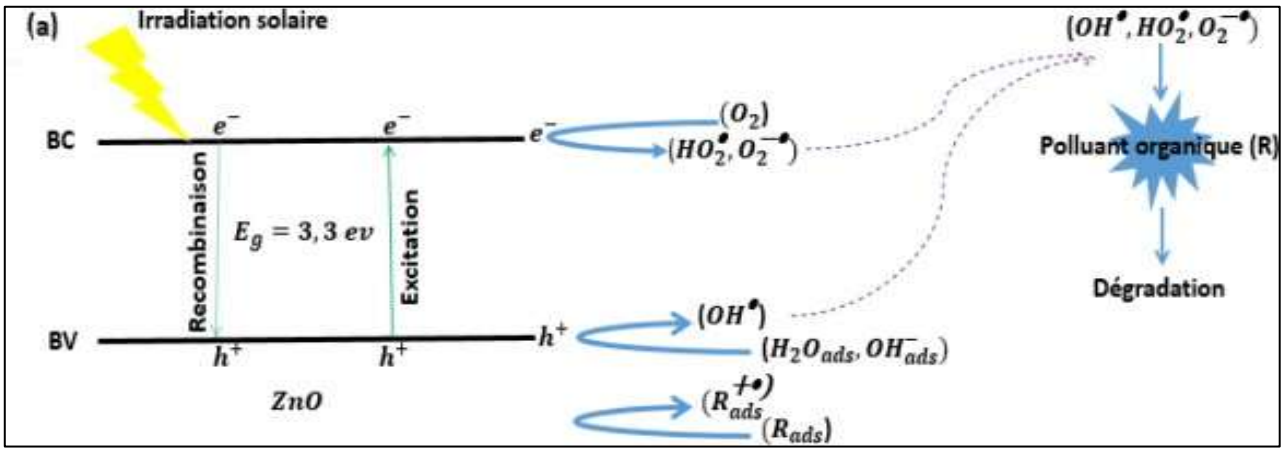


Figure 6. Schematic energy band diagram and proposed photocatalytic mechanism of ZnO NPs under solar irradiation, showing generation of electron-hole pairs, reactive oxygen species (OH•, HO2•, O2•-), and mineralization of the organic pollutant (MB).

**4.2 Antibacterial Activity**

The antibacterial efficacy of the synthesized ZnO NPs was evaluated against four reference bacterial strains by the agar disk diffusion method. The inhibition zone diameters are summarized in Table 1, and representative photographs of the inhibition zones are shown in Figure 7.

Table 1. Inhibition zone diameters (mm) of ZnO NPs against tested bacterial strains

| Bacterial Strain | Gram Type | Inhibition Zone (mm) | Classification |
|---|---|---|---|
| **E. coli** | Gram-negative | 35 | High activity |
| **P. acip** | Gram-negative | 23 | Moderate activity |
| **S. aureus [ATCC 25932]** | Gram-positive | 0 | No activity |
| **S. aureus [ATCC 43300]** | Gram-positive | 15 | Moderate activity |

The ZnO NPs demonstrated the highest antibacterial activity against Gram-negative bacteria: E. coli (35 mm) and P. acip (23 mm), while showing moderate inhibition against Gram-positive S. aureus ATCC 43300 (15 mm) and no detectable activity against S. aureus ATCC 25932 (0 mm).

The superior susceptibility of Gram-negative bacteria can be explained by the structural differences in their cell walls. Gram-negative bacteria possess a thin peptidoglycan layer (˜2–7 nm) sandwiched between the outer membrane and inner plasma membrane, which allows easier penetration of ZnO NPs and their released Zn2+ ions into the bacterial cell interior, leading to disruption of metabolic processes and cell death [9, 14]. In contrast, Gram-positive bacteria such as S. aureus have a thick, multilayered peptidoglycan cell wall (˜20–80 nm) that provides a more effective physical barrier against nanoparticle penetration.

The antibacterial mechanism of ZnO NPs involves multiple synergistic pathways: (i) generation of ROS that cause oxidative damage to cell membranes, proteins, and DNA; (ii) direct physical contact and membrane disruption; and (iii) intracellular release of Zn2+ ions that interfere with enzymatic activity [9, 15]. These results are consistent with those reported for ZnO NPs synthesized from Pelargonium odoratissimum (IC50 = 28.11 μg/mL, inhibition zones 15–22 mm) [16] and from Oxalis stricta leaf extract [3].

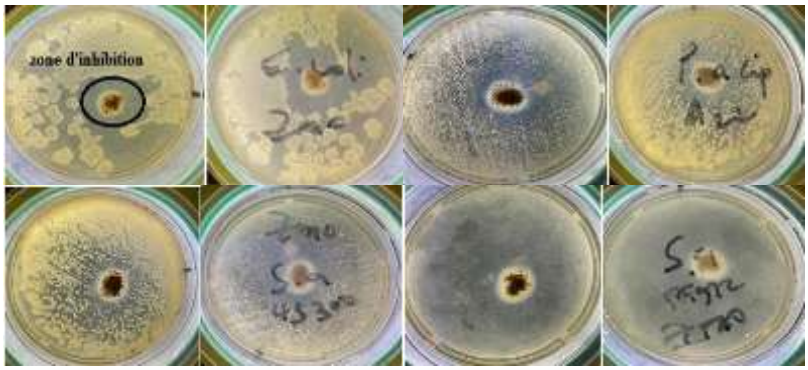


Figure 7. Digital photographs showing inhibition zones produced by ZnO NPs against (top-left) E. coli showing a clear inhibition halo, (top-right) P. acip, (bottom-left) S. aureus ATCC 43300, and (bottom-right) S. aureus ATCC 25932 (no inhibition zone).

**4.3 Antioxidant Activity (DPPH Assay)**

The antioxidant potential of ZnO NPs was assessed using the DPPH free radical scavenging assay and compared against ascorbic acid (AA) as a positive reference (Figure 8). The DPPH assay measures the ability of the tested material to donate hydrogen atoms or electrons to the stable DPPH• radical, causing a characteristic color change from violet to yellow, which is monitored spectrophotometrically.

The results show that ZnO NPs exhibit concentration-dependent DPPH radical scavenging activity, reaching approximately 70% inhibition at 10 mg/mL. The calculated IC50 value for ZnO NPs was 9.5 mg/mL, compared to 0.033 mg/mL for ascorbic acid, indicating that the nanoparticles possess moderate antioxidant activity, significantly lower than the vitamin C reference. These findings are in agreement with previous studies on biogenic ZnO NPs: Abdelbaky et al. [16] reported IC50 = 28.11 μg/mL for P. odoratissimum-derived ZnO NPs, and Mentha piperita-based ZnO Bio NPs inhibited 52% of DPPH radicals at 15.63 μg/mL [6], with performance differences attributable to variations in particle size, surface area, and residual phytochemical coating.

The antioxidant activity of ZnO NPs is attributed to the combined effect of residual surface-bound phytochemicals from the plant extract—particularly polyphenols such as rosmarinic acid and flavonoids—and the intrinsic radical scavenging properties of the ZnO surface through electron transfer mechanisms. The

moderate activity observed suggests that while ZnO NPs may not replace dedicated antioxidants like ascorbic acid in pharmaceutical applications, they can contribute to protective effects in composite formulations [13, 16].

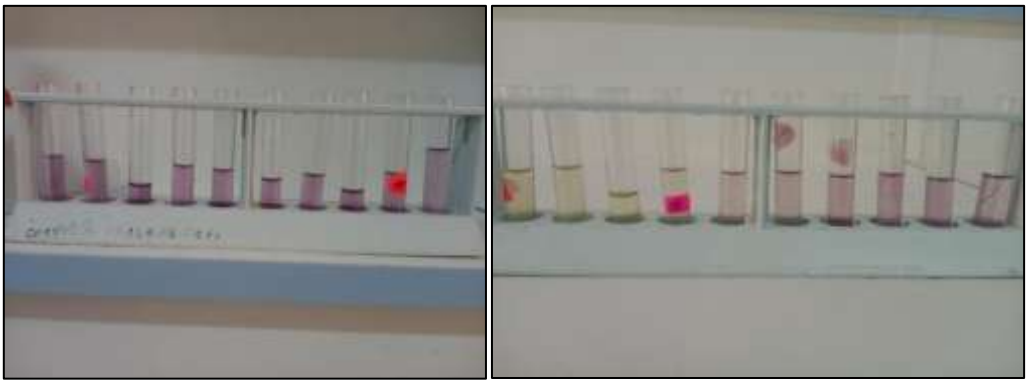

Figure 8. Photographs showing DPPH radical scavenging assay results for ZnO NPs (left: initial violet color at various concentrations; right: progressive decolorization indicating antioxidant activity with increasing ZnO NP concentration versus ascorbic acid control).

## 5. CONCLUSION

This study successfully demonstrates the green synthesis of ZnO nanoparticles using an aqueous extract of Mentha aquatica leaves as an eco-friendly, cost-effective bio-reducing and capping agent. The synthesized ZnO NPs were thoroughly characterized by UV-Vis, FTIR, XRD, and SEM techniques.

UV-Vis spectroscopy confirmed the characteristic absorption band at ~380 nm, indicative of ZnO formation. FTIR analysis revealed the role of phenolic hydroxyl and carbonyl groups from the plant extract in reducing $Zn^{2+}$ ions and stabilizing the nanoparticle surface. XRD patterns verified the hexagonal wurtzite structure with high crystallinity (JCPDS 36-1451), and Scherrer analysis yielded a crystallite size of 16–22 nm, corroborated by SEM morphological observations of spherical-to-granular particles.

The ZnO NPs demonstrated excellent photocatalytic degradation of methylene blue under natural solar irradiation, achieving near-complete decolorization within 120 min through a mechanism involving generation of hydroxyl radicals and superoxide species. Strong antibacterial activity was recorded against Gram-negative E. coli (35 mm) and P. acip (23 mm), explained by the thinner cell wall of these organisms facilitating nanoparticle internalization. Moderate antioxidant activity was determined with an IC50 of 9.5 mg/mL by the DPPH assay.

These multifunctional properties establish Mentha aquatica-derived ZnO NPs as promising candidates for environmental (photocatalytic dye removal), biomedical (antimicrobial coatings and formulations), and nutraceutical (antioxidant composite) applications. Future work should focus on scale-up optimization, mechanistic studies of the bioreduction process, and in vivo biocompatibility assessment.

**REFERENCES**

[1] Alharbi, F.N., Abaker, Z.M., & Makawi, S.Z.A. (2023). Phytochemical substances-mediated synthesis of zinc oxide nanoparticles (ZnO NPs). Inorganics, 11(8), 328. https://doi.org/10.3390/inorganics11080328

[2] Govindasamy, R., et al. (2024). Green synthesis of Mn-doped ZnO nanoparticles using Ipomoea staphylina leaf extract: Characterization and application of photocatalytic dye degradation, antibacterial and antioxidant activity. ChemistrySelect, 9. https://doi.org/10.1002/slct.202402347

[3] Han, Q., et al. (2023). Green-synthesized ZnO nanoparticles from plant extracts: Characterization, photocatalytic activity, and antibacterial activity. Ionics, 29, 5095–5110. https://doi.org/10.1007/s11581-025-06849-2

[4] Nanomaterials (2024). A review of plant-mediated ZnO nanoparticles for photodegradation and antibacterial applications. Nanomaterials, 14(14), 1182. https://doi.org/10.3390/nano14141182

[5] Scientific Reports (2024). Enhanced photocatalytic activity of green synthesized zinc oxide nanoparticles using low-cost plant extracts. Scientific Reports, 14, 16713. https://doi.org/10.1038/s41598-024-66975-1

[6] Freitas, C.S., et al. (2025). Eco-friendly synthesis and biomedical potential of zinc oxide nanoparticles using Mentha piperita aqueous extract: comparative analysis with chemically synthesized and commercial nanoparticles. Bioprocess and Biosystems Engineering. https://doi.org/10.1007/s00449-025-03178-6

[7] Dhiman, S., et al. (2023). Green nanotechnology advances: green manufacturing of zinc nanoparticles using Mentha spicata (mint) and Ocimum basilicum (basil) leaf extracts. Environmental Science and Pollution Research. https://doi.org/10.1007/s11356-023-26827-3

[8] Aldeen, T.S., Mohamed, H.E.A., & Maaza, M. (2022). ZnO nanoparticles prepared via a green synthesis approach: Physical properties, photocatalytic and antibacterial activity. Journal of Physics and Chemistry of Solids, 160, 110313.

[9] Celosia cristata study (2023). Investigation of antibacterial and photocatalytic efficiency of green ZnO nanoparticles synthesized with Celosia cristata flower extract. PMC. NCBI PMC10734710.

[10] Fakhari, Shabnam, Mina Jamzad, and Hassan Kabiri Fard. "Green synthesis of zinc oxide nanoparticles: a comparison." Green chemistry letters and reviews 12.1 (2019): 19-24.

11] Yılmaz, A., et al. (2023). Photocatalytic and antibacterial activities of ZnO nanoparticles synthesized from Lupinus albus and Lupinus pilosus plant extracts via green synthesis approach. Spectrochimica Acta Part A, 301, 122974. https://doi.org/10.1016/j.saa.2023.122974

[12] UdayachandranThampy, U., et al. (2019). Enhanced photocatalytic activity of ZnO–NiO nanocomposites synthesized through a facile sonochemical route. SN Applied Sciences, 1, 1–15.

[13] Sugitha, S.K.J., et al. (2024). Green synthesis of Al-ZnO nanoparticles using Cucumis maderaspatanus plant extracts: analysis of structural, antioxidant, and antibacterial activities. Nanomaterials, 14(22), 1851. https://doi.org/10.3390/nano14221851

[14] Mondal, S.K., et al. (2024). Antimicrobial nanoparticles: Current landscape and future challenges. RSC Pharmaceutics, 1(1), 388–402.

[15] Catunaregam spinosa study (2024). Green synthesis of zinc oxide nanoparticles using Catunaregam spinosa for biological applications. PMC.

[16] Abdelbaky, A.S., et al. (2022). Green synthesis and characterization of ZnO nanoparticles using Pelargonium odoratissimum (L.) aqueous leaf extract and their antioxidant, antibacterial and anti-inflammatory activities. Antioxidants, 11(8), 1444. https://doi.org/10.3390/antiox11081444